Theor Chim Acta (1993) 85: 285–303

Theoretica Chimica Acta

Optimization of both resonance structures of the glyoxal radical cation by means of the Valence Bond Self-Consistent Field method

J. H. Langenberg and P. J. A. Ruttink

Theoretical Chemistry Group, University of Utrecht, Padualaan 14, NL-3584 CH Utrecht, The Netherlands

Received May 8, 1992/Accepted June 10, 1992

Summary. The Valence Bond Self-Consistent Field (VBSCF) method is used to form various wave functions of distinct quality, in which the resonance structures of the glyoxal radical cation are explicitly present. These wave functions are fully optimized, and the corresponding total energies are calculated for several nuclear geometries of the ion. It is shown that the potential energy surfaces of the VBSCF functions are continuous on symmetry lowering, whereas RHF and CASSCF surfaces expose gaps. Localization of the unpaired electron either on both oxygen atoms, in case of C_{2h} symmetry, or on a single oxygen atom, in case of C_s symmetry, is well described by the VBSCF functions, and a smooth transition between the two states is obtained.

Key words: Symmetry breaking – Resonance structures – Valence Bond Self-Consistent Field – Breathing orbitals – Molecular switches

1 Introduction

The glyoxal molecule O(H)C–C(H)O is representative of a class of molecules containing equivalent sites that have the potency of carrying charge. If such a molecule is ionized, the charge – or more accurately the unpaired electron – may either be localized on one of the sites, causing a lowering of the symmetry of the molecular skeleton, or it may be delocalized, in which case symmetry will be retained. An example of the first possibility is the chinon molecular cation $O{=}C_6H_4{=}O^{+\cdot}$ [1], whereas the second possibility holds e.g. for $O^{2+\cdot}$ [2]. The glyoxal radical cation $[O(H)C{-}C(H)O]^{+\cdot}$ is a special case since according to RHF calculations both possibilities seem to be present. Using a SV 4-31G basis, the trans isomer appears to have two minima in its potential energy surface: one with $R_{CC} \approx 1.5$ Å of C_s symmetry (and its inverted equivalent) and another with $R_{CC} \approx 2.1$ Å of C_{2h} symmetry. The charge in the first minima is localized, whereas the charge in the last minimum is delocalized. The minima of lowest symmetry are global. The potential energy surface is continuous where the C–C distance is large, but for instance at $R_{CC} = 1.5$ Å the C_{2h} constrained solution appears to be unstable. This discontinuity makes molecular geometry predictions based on the RHF surface unreliable.

The observation that RHF shows preference for localization in a competition between a "localized" and a "delocalized" situation has been made many times, and its underlying principles have been thoroughly studied [3–9]. It is brought about by the fact that the delocalized state is much harder to describe, since this involves localization at different equivalent sites, whereas the radical character must not be smeared out over the chain of atoms connecting these sites. In fact, the state is more correctly characterized by the term "multiple-localized". A wave function that is to represent such a state properly should incorporate all corresponding resonance structures, which is impossible for a 1-configuration optimization. For the "mono-localized" situation one resonance structure suffices, and RHF is good enough. However, in the treatment of a system of which it is not quite clear which situation is favoured, a procedure is required that deals well with both situations. Several more sophisticated methods than RHF also seem to lack this ability: In Multi-Reference SDCI calculations on the glyoxal ion [10], the two distinct Pople corrections for size consistency [11] appeared to differ enormously: 10 kcal mol^{-1}. This indicates that the 2-configuration reference function, used in these calculations, is not a proper zeroth order wave function for the ion. Even appliance of Complete Active Space SCF, generally considered good enough to deal with all non-dynamical correlation, remained without success [12].

The difficulties encountered by RHF and the above methods forced us to look for a less established procedure to apply to our ion. The above analysis of what a wave function should be able to contain naturally brings forward Valence Bond as a possible alternative. There are several existing Valence Bond methods with which resonance structures can be incorporated directly in the wave function [13]. These can all be classified under non-orthogonal CI. The choice of both the orbital optimization preceding the CI and the selection of the resonance structures differs per method. Broer and Nieuwpoort [14] start off with a symmetry broken RHF solution. They then gather by symmetry projections all remaining broken solutions to perform subsequently a non-orthogonal CI. Hollauer and Nascimento [15–17] have recently introduced a method that may be considered as an extension of the former approach: Before being subjected to a non-orthogonal CI, the parts of the wave function representing resonance structures are optimized separately on an arbitrary level of approximation. They call their procedure Generalized Multistructural (GMS) description. However, neither of these methods reoptimizes the orbitals for the final multiconfigurational wave function, and here we arrive at what forms the novelty of our approach: *We use the Valence Bond Self-Consistent Field (VBSCF) method to incorporate resonance structures explicitly in the wave function, and optimize them simultaneously.* In the most sophisticated approach we will present, the resonance structures – each represented by a single configuration – are given full flexibility at the orbital level.

In a detailed analysis of discontinuity on CASSCF surfaces by De Meras et al. [18], the behaviour of the CASSCF optimization is explained in terms of two opposing forces: polarization and resonance. It is here concluded that the lowest CASSCF solution will be symmetry broken if the resonance energy between the structures is less than twice the polarization energy. We feel that the reason that this condition is so often fulfilled is because orthogonal configurations are used to define the resonance structures. The demand to keep the configurations orthogonal reduces the resonance energy. Releasing this constraint allows for a better account of the resonance phenomenon resulting in an optimization during which the two opposing forces – polarization and resonance – are truly balanced.

To our knowledge, no detailed account of the glyoxal radical cation has thus far been presented. Some research has however been done on excited states [19, 20] of the neutral glyoxal molecule and on its ionization potentials [15]. In the calculation of both quantities the same kind of symmetry dilemma is encountered as with the ion and all authors stress the need for localized descriptions. Hollauer and Nascimento [15] use the above mentioned GMS description to obtain this. Solving the symmetry related problems evoked by the glyoxal ion is not of mere academic interest: Actually, it may be of importance in the field of molecular switches [21, 22]. Here, one searches for molecules that can localize charge on equivalent "left" or "right" sides, these sites being separated by a barrier of a specific height. There are indications that the potential energy surface of the glyoxal ion shows just the appropriate shape, and forms thus an interesting study case – at least from the theoretical point of view.

Section 2 introduces three model VBSCF functions that differ in the flexibility allowed to the individual configurations. The freedom allowed on the orbital level leads to the introduction of a new terminology, that of "breathing orbitals". Analysis of optimized VBSCF functions, in Sect. 3, shows how they resemble resonance structures. By showing the orthogonal analogue of a VBSCF function and by including CASSCF and non-orthogonal CI calculations, in Sect. 4, we give an idea of how the VBSCF method – as we use it – should be judged compared to other "better than SCF" methods. In Sect. 5 we study part of the potential energy surface of the glyoxal ion, using RHF, CASSCF, and VBSCF functions. The main aim of these calculations is to show that, unlike RHF and CASSCF functions, the VBSCF functions are stable with respect to symmetry changes over a wide range of the C–C distance. Though some conclusions concerning the geometry of the ion are drawn, a rigorous exploration of its ground state surface falls beyond the scope of this investigation. Section 6 summarizes our results. The standard SV 4-31G basis set [23] is used in all calculations.

2. Formal VBSCF functions for the glyoxal radical cation containing breathing orbitals

Balint-Kurti and van Lenthe [24, 25] devised the VBSCF method and performed some test calculations, whereafter Verbeek modified it [26–29] and developed a state-of-the-art implementation [30]. Here, we give only a brief characterization of the method. Basically, the VBSCF method is a Multi-Configuration SCF method that allows for the use of non-orthogonal orbitals. The VBSCF function is formed by a linear combination of Valence Bond structures, i.e. spin projections of orbital configurations. Unlike other Valence Bond methods, the VBSCF method puts no restrictions upon the number of configurations, the orbital occupation numbers, and the number of structures (spin functions) per configuration. It is thus a very general optimization method. TURTLE, code name of our VBSCF implementation, leaves it up to the user to design a formal wave function. Whether this wave function can be optimized or not will be revealed in the course of a calculation; it forms the ultimate test whether the chosen model makes sense or not. The orbitals that form the building blocks of the wave function can be restricted to be fully localized, though this is not required. Often they are centred at a certain atom but slightly distorted towards a neighbour. There are also orbitals that resemble a localized bonding. In our study, orbitals have no constraints, but they are nevertheless sufficiently localized to paste

(inter-)atomic labels on them. A warning is in place, however, since the shape of orbitals can not always be interpreted physically; for instance, the localization of inactive orbitals has no significance at all [26]. Note that spin-coupling does not occur in our wave functions, as we will use only one single occupied orbital per configuration.

In the following, we will develop formal wave functions for a glyoxal ion missing an n-electron, which are of uniform quality with respect to alteration of the symmetry of the nuclear skeleton. In selecting configurations for this wave function we are guided by the Lewis structures of the ion. Two resonance structures can be formed; each has the unpaired electron located at a different oxygen atom (see Fig. 1).

The quantum chemical equivalent of the resonance structure model is formed by a 2-configuration VBSCF function. This wave function contains so called breathing orbitals [31], which will be defined below. In the following, N will refer to the number of electrons and parenthesized figures will refer to orbital occupation numbers. The z-axis will lie in the plane of the molecule, rectangular to the O–C bonds (see Fig. 1). Suppose we take two configurations, each consisting of $(N-3)/2$ closed shells and 2 variable occupied ("active") localized oxygen orbitals, say O_{pz}, which contain the remaining 3 electrons. Labeling the left and right oxygen p_z orbitals L and R respectively, yields O^L_{pz} and O^R_{pz}. If the active orbitals in the two configurations are allowed to respond to their occupation number, the O^L_{pz}-orbital (and the O^R_{pz}-orbital) in the first structure will be different from that in the second. We will call an orbital that is allowed to be different in each configuration a "breathing orbital". To provide each resonance structure with such flexibility has been proposed by e.g. Voter and Goddard [32].

We will use 4 types of optimization schemes, which differ in the breathing capacity of the wave functions (see Table 1). All types consist of two configurations, which are equally weighted in case of C_{2h} symmetry. First we shall demonstrate the most primitive representation of the Lewis structures of the ion. Assuming that the closed shell orbitals are the same in both configurations, and showing active orbitals only, its configurations are:

$$O^L_{pz}(1)O^R_{pz}(2) \quad \text{and} \quad O^L_{pz}(2)O^R_{pz}(1) \qquad \text{"0"}$$

This wave function will be referred to as "type 0". The two structures can be interconverted by single excitation, and so, according to the Brillouin theorem, type 0 can not be expected to have more degrees of freedom than a 1-configuration

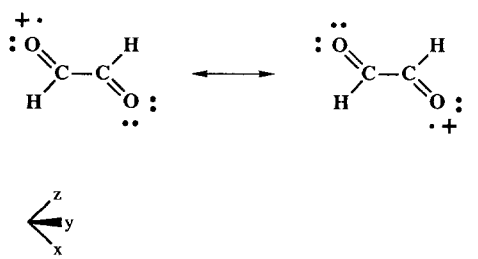

Fig. 1. Lewis structures of the glyoxal radical cation

Table 1. Breathing capacity specifications for 2-configuration VBSCF functions[a]

Type	Breathing orbital groups	Number of breathing orbitals
0		0
1	O_{pz}	2
2	$O_{pz}O_{2s}\sigma_{OC}$	6
3	$O_{pz}O_{2s}\sigma_{OC}\pi_{OC}\sigma_{CH}\sigma_{CC}$	11

[a] A breathing orbital is defined as an orbital that is represented by distinct orbitals in different configurations. The various "representatives" corresponding to a breathing orbital are thus unequal, though localized in the same molecular space. Each breathing orbital group, except the central σ_{CC} group that has only one member, consists of two breathing orbitals; one localized in the left and one localized in the right part of the molecule

wave function. A great improvement is made when we allow the active orbitals to breathe. We then arrive at the following configurations:

$$O_{pz}^{L'}(1)O_{pz}^{R''}(2) \quad \text{and} \quad O_{pz}^{L''}(2)O_{pz}^{R'}(1) \qquad \text{"1"}$$

The O_{pz}^{L}- and O_{pz}^{R}-orbitals in "type 1" are the breathing orbitals defined above. To put it differently, a breathing orbital can be thought of as an orbital that has distinct "representatives" in different configurations.

In type 1 only the (variable occupied) O_{pz}-orbitals are allowed to breathe. In this case the two configurations still share a "sea" of double occupied orbitals, which necessarily reflects the symmetry of the entire molecule. This symmetrical sea might hinder the breathing orbitals in their respective localizations of the unpaired electron. This can be remedied if we define extensions to type 1 in which more orbitals are allowed to breathe, ultimately leading to two structures that are given full flexibility to respond to their respective localizations of the unpaired electron. Thus, we also define "type 2" that has some orbitals centred at or near the oxygen atoms breathing, and finally "type 3" that has all orbitals (except C_{1s} and O_{1s}) breathing. (See Table 1.) Type 0 contains no breathing orbitals and is obviously just an unusual representation of the RHF function. Still it provides a good starting point from the conceptual point of view for the more sophisticated models. It may be expected that type 1 essentially contains the additional flexibility needed to describe the localization of the charge. The other types may be regarded as further improvements, which, however, will yield qualitatively the same results as type 1.

Note the special way in which symmetry is dealt with: Recall that all orbitals are localized in the sense described previously and suppose a C_{2h} nuclear framework. Then, for each orbital in the "left" configuration (except for the central σ_{CC}) there exists an equivalent one in the "right" configuration; the latter obtainable by performing a symmetry operation, rotation over C_2 axis, on the former [26]. (To illustrate this, we have related equivalent orbitals in our definition of type 1 by giving them equal numbers of primes.)

3 Characteristics of the optimized VBSCF functions

In this section, we apply full orbital optimization to the 2-configuration VBSCF functions defined in the previous section and discuss the merits of the optimized wave functions. No orthogonality *restrictions* are applied during the optimization, though orthogonalization of orbitals is automatically invoked wherever this leaves the wave function unaltered. The calculations are performed at the C_{2h} RHF-optimized geometry of the glyoxal ion. Note that this geometry is characterized by an exceptionally long C–C bond length (2.05 Å). The groundstate of the ion in C_{2h} symmetry is A_g. To gain some insight into the charge and spin distribution of the VBSCF functions, we show Mulliken populations of optimized wave functions and of individual configurations.

In Table 2 we present total energies and timings for all introduced types. By allowing the active orbitals to respond to their occupancy 14 mH is gained, and permitting full flexibility to the doubly occupied MO's yields another 20 mH. The "intermediate breathing" wave function, type 2, lies halfway between type 1 and 3.

The Mulliken atomic charge and spin populations of optimized wave functions and the configurations they're composed of, are presented in Table 3. The populations are calculated from the 1-electron density matrix [26]. Within the configurations the unpaired electron is located mainly at one of the oxygen atoms, whereas the charge and spin distribution in the full wave functions is symmetrical. So in all types both resonance structures of the ion are represented in equal proportions. However, if we take a better look at the overall "distribution" of the unpaired electron, we notice a clear difference between type 0 and the other types: *Without breathing orbitals the radical character is distributed evenly over the* O–C–C–O *axis, whereas for the other wave functions it is substantially localized at the oxygen atoms.* As the level of breathing is increased, this localization becomes more pronounced, but the main effect lies in the allowance for breathing of the variable occupied orbitals. In going from the charge populations for type 0 to type 3 wave functions, we spot a weak tendency towards a spread of the charge over the molecule. The populations of the type 0 (2-configuration) function equal those of RHF (not shown), definitively proving that the former is just a transformation of the latter.

Table 2. VBSCF calculations at the glyoxal ion[a]

Type	Total energy (a.u.)	CPU seconds[b]
0	−225.865669	7000 (40)[c]
1	−225.879909	3000
2	−225.890667	10000
3	−225.900489	11000

[a] Nuclear geometry corresponds to the C_{2h} constrained RHF minimum

[b] Apollo DN 10000

[c] Type 0 suffers from intrinsic convergence difficulties (see text). The number within parenthesis gives the timing of a RHF calculation that leads to equivalent results

Table 3. Mulliken atomic charge (A and B) and spin (C and D) populations for optimized 2-configuration VBSCF functions (B and D) and "left" configurations (A and C) taken from these functions

	Atom	Type			
		0	1	2	3
A	O	7.85	7.87	7.93	7.99
	O	8.43	8.46	8.39	8.35
	C	5.88	5.90	5.81	5.78
	C	5.59	5.51	5.60	5.62
	H	0.60	0.61	0.62	0.59
	H	0.65	0.65	0.65	0.66
B	O	8.25	8.23	8.22	8.21
	O	8.25	8.23	8.22	8.21
	C	5.65	5.67	5.68	5.68
	C	5.65	5.67	5.68	5.68
	H	0.60	0.60	0.61	0.61
	H	0.60	0.60	0.61	0.61
C	O	0.61	0.74	0.74	0.79
	O	0.03	0.04	0.07	0.02
	C	0.01	0.01	0.00	0.00
	C	0.30	0.19	0.18	0.16
	H	0.05	0.03	0.02	0.02
	H	0.00	0.00	0.00	0.01
D	O	0.20	0.33	0.34	0.36
	O	0.20	0.33	0.34	0.36
	C	0.25	0.13	0.12	0.10
	C	0.25	0.13	0.12	0.10
	H	0.05	0.04	0.04	0.03
	H	0.05	0.04	0.04	0.03

Note that the configurations also show considerable surplus alpha spin on the carbon atom that takes the β-position to the "ionized" oxygen atom. This is understandable in regard of the long C–C bond length. Utilizing the fact that in the current geometry the ion is nearly dissociating along the C–C axis, extra resonance structures can be drawn that explain the radical character at the β-position, see Fig. 2.

Finally, we present overlap integrals between the two representatives of each breathing orbital (Table 4). If we interpret orbital-overlap as a measure of the "likeness" of two orbitals, the difference between the representatives of the breathing orbitals looks surprisingly small, considering the substantial energy lowering accompanying breathing. The exceptional length of the C–C bond probably brings about the comparably small overlap between the representatives of the central σ_{CC}-orbital.

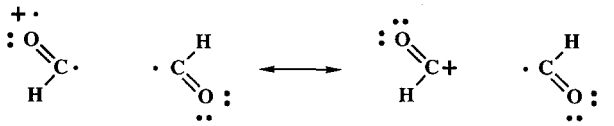

Fig. 2. "Left" Lewis structures of the glyoxal ion for dissociation along the C–C axis

Efforts to allow the 1*s* carbon and oxygen orbitals to breathe as well failed. In the split valence basis set the overlap between the two representatives of the 1*s* breathing orbitals would probably be too close to unity. In this case, the splitting of these orbitals into different representatives is in vain and does in practice lead to linear dependencies.

4 Comparison of VBSCF with other methods

The 2-configuration VBSCF functions, that were shown in the previous section to resemble closely the glyoxal ions resonance structures, can only be optimized by releasing orthogonality restrictions. Considering the overlaps between representatives of the various breathing orbitals (Table 4), it is unthinkable that any conventional 2-configuration MCSCF function will carry the same properties as the VBSCF functions. It is however possible to convert the VBSCF functions to orthogonal equivalents. These equivalents consist of much more configurations than just 2. In fact, they appear to be complete active space expansions of $2n-1$ electrons in $2n$ (orthogonal) orbitals with fixed CI coefficients, n being the number of breathing orbitals. For type 1 this wave function consists of 20 CSF's instead of 2. The size of the expansions increases explosively with the number of breathing orbitals: Type 2 corresponds to a "contracted" 11 in 12 CAS expansion, that is 339 768 CSF's, whereas type 3 corresponds to a contracted 21 in 22 CAS expansion: 2.3×10^{11} CSF's!

Of course, the contracted CI functions are neither optimized to CI coefficients, nor to orbitals. Therefore, starting from the orthogonal equivalent of type 1, we optimize both coefficients and orbitals (CASSCF) and coefficients only (CASCI) to see to what extent the orthogonalized wave function is optimized by the generating VBSCF procedure. The active space in the CAS

Table 4. Overlap integrals between representatives of breathing orbitals

Breathing orbital groups	Type		
	1	2	3
O_{pz}	0.952	0.915	0.887
O_{2s}		0.988	0.985
σ_{OC}		0.992	0.991
π_{OC}			0.994
σ_{CH}			0.986
σ_{CC}			0.711

calculations is defined as follows: The reference function contains two active orbitals, one is singly occupied ($7a_g$) and another is doubly occupied ($6b_u$). There are two active virtuals ($8a_g$ and $7b_u$). The configurations are obtained by performing all possible excitations from the occupied actives in the reference configuration to the active virtuals, neglecting those that lead to symmetry forbidden configurations. Total energies for these calculations can be found in Table 5. They form numerical evidence for the fact that the CASCI and CASSCF calculations have more degrees of freedom than the VBSCF calculation, but they also show that the active space is reasonably exploited by the VBSCF optimization.

The larger contracted expansions are virtually impossible to realize, which pleads for the VBSCF method. Though CASSCF calculations, with less configurations than the contracted expansions shown here, can yield lower total energies, the VBSCF functions (and thus their orthogonal equivalents) will next prove to have some qualities that are of extreme value in symmetry examining calculations. Releasing orthogonality constraints clearly makes it much easier to attain these qualities.

For small C–C distances, C_{2h} constrained RHF solutions are not stable with respect to symmetry reduction. A well-tried approach to obtain symmetry adapted wave functions out of broken ones is to perform a non-orthogonal CI calculation between all broken solutions [14]. One broken solution is sufficient to generate the complementary ones, since all broken solutions are interconvertible by symmetry operations. In Table 6 we compare the outcome of such a calculation, loosely referred to as "VBCI", with our VBSCF results. The chosen geometry has a C–C bond length of 1.6 Å, short enough for RHF to prefer

Table 5. Relaxation of the orthogonal equivalent of type 1

Method	Total energy (a.u.)
Type 1/Contracted CI	−225.879908
CASCI	−225.888859
CASSCF	−225.890019

Table 6. Comparison of VBSCF with RHF and non-orthogonal CI between broken RHF solutions ("VBCI")

Method	Total energy (a.u.)
RHF[a]	−225.854492
RHF[b]	−225.863808
Type 1[c]	−225.876595
VBCI	−225.887055
Type 2[c]	−225.892949
Type 3[c]	−225.915408

[a] Symmetry adapted solution
[b] Symmetry broken solution
[c] VBSCF calculation

symmetry breaking. Out of a symmetry broken RHF solution a complementary wave function is created by rotation of the orbitals of the first one over the C_2 axis. The two broken solutions define a two by two non-orthogonal CI problem. The VBCI energy lies below type 1. However, the sequence in Table 6 is somewhat arbitrary as the energy of the VBCI calculation relative to the VBSCF calculations is likely to depend rather strongly on the C–C distance (at a certain distance the lowest RHF solution becomes C_{2h} adapted). In any case it is safe to say that type 3 will always lie below VBCI, since the former contains the same number of broken orbitals as the latter but has all its orbitals optimized. The VBCI method is orders of magnitude faster than VBSCF, and it may seem a preferable method. However, for C_s symmetry the C_2 rotation is no longer a symmetry operation, and the VBCI configurations can no longer be uniquely defined. Consequently, this procedure is of no use in comparing parts of the potential surface that are of different symmetry, which is essential in our study of the glyoxal ion.

5 The potential energy surface of the glyoxal radical cation

In this section we sketch the RHF, CASSCF, and VBSCF surfaces of the glyoxal ion. Furthermore, we perform a test to see whether these surfaces contain discontinuities. The SV 4-31G basis set [23] is used throughout. Both RHF and CASSCF calculations were performed using the GAMESS program package [33–35].

As mentioned in the introduction, the RHF potential energy surface is characterized by some peculiar features. We will treat this surface in more detail now. A schematic overview is shown in Fig. 3. The capitals on the figure mark geometries at which VBSCF calculations are performed, these will be treated hereafter.

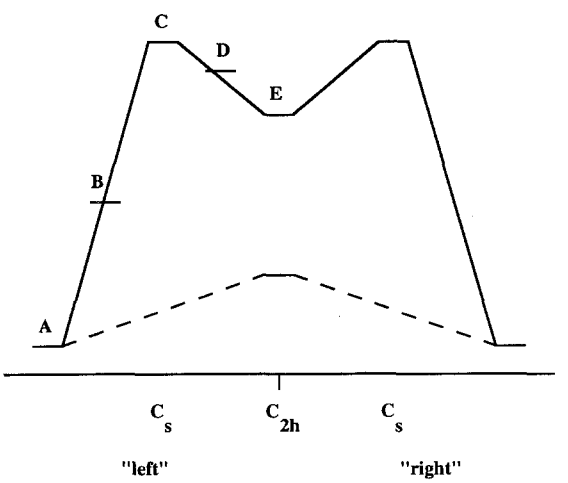

Fig. 3. Schematic representation of the RHF potential energy surface of the glyoxal ion. The letters mark nuclear geometries used in calculations: A is one of the global C_s minima, C one of the saddle points (C_s), E the C_{2h} local minimum. B lies geometrically between A and C, whereas D lies between C and E. Connected by dashed lines to the C_s global minima, lies the lowest symmetry broken point at a C_{2h} geometry

There are two equivalent global minima of low symmetry. The calculated bond length for the skew minima (1.53 Å) is reasonable regarding the bond length in the neutral molecule (1.49 Å, in a SCF-optimized geometry). C_{2h} constrained geometry optimization leads to an unusually large C–C distance: 2.05 Å. In this region of the surface, symmetry adaption is no constraint, and the optimized geometry forms a true local minimum. The unpaired electron is smeared out over the entire O–C–C–O skeleton, as was concluded in Sect. 3, from Table 3D.

The C_s minima are mono-localized. In the atomic spin population this shows by the fact that the contributions involving the oxygen atom are as large as 0.91. The skew minima are separated from the local C_{2h} minimum by saddle points, which are characterized by huge imaginary frequencies: 2277i cm^{-1}. The saddle points mark the border on the surface between the localized and the delocalized (and not multiple-localized!) region. For shorter C–C distances, C_{2h} constrained RHF solutions are no longer stable. In fact, if we symmetrize the internal coordinates of a C_s minimum and generate a symmetry broken solution at this geometry, the corresponding energy lies below the symmetry adapted minimum. We will return to the phenomenon of symmetry breaking hereafter. Details considering the geometry and the energetics of the surface are found in Tables 7 and 8. (The ascription of local minima and saddle points was affirmed by performing force constant calculations, both for the RHF and the CASSCF surface.)

The active space of the 3 in 4 CASSCF calculations, presented in this paper, was defined in Sect. 4, at least for C_{2h} symmetry. For C_s symmetry, the active space of the A′ wave function consists entirely of a' orbitals. The CASSCF surface is shown schematically in Fig. 4. Total energies at the stationary points of this surface are presented in Tables 9 and 10.

The CASSCF potential energy surface has some features in common with RHF. There are two local C_s minima with acceptable (short) C–C bond lengths, which are separated from the large C–C distance region by saddle points. Furthermore, for short C–C distances, C_{2h} constrained solutions appear to be unstable. However, if we take a closer look at the large C–C distance region, we discover a rare topology. Even for $R_{CC} = 2.05$ Å, symmetry adapted solutions at C_{2h} geometries are unstable. We find two *global* C_s minima in this area, *which are very close to* C_{2h} *symmetry*. (Left and right bond lengths and angles differ no more than 0.004 Å and 4°, respectively.) The global minima lie only 0.1 mH

Table 7. Stationary points at the RHF potential energy surface

Symmetry	Total energy (a.u.)
C_s [a]	−225.876204
C_s [b]	−225.863049
C_{2h} [c]	−225.865671
C_{2h} [d]	−225.873184

[a] Global minimum
[b] Saddle point
[c] Symmetry adapted local minimum
[d] Symmetry broken minimum

Table 8. Bond lengths and bond angles (Ångstrom/degrees) at RHF stationary points

	C_s [a]	C_s [b]	C_{2h} [c]
R_{CC}	1.535	1.870	2.053
R_{CO1}	1.192	1.146	1.141
R_{CO2}	1.233	1.164	1.141
R_{CH1}	1.074	1.077	1.082
R_{CH2}	1.084	1.085	1.082
θ_{CCO1}	114.8	113.1	112.8
θ_{CCO2}	121.8	116.0	112.8
θ_{CCH1}	118.1	107.2	104.3
θ_{CCH2}	120.4	112.3	104.3

[a] Global minimum
[b] Saddle point
[c] Symmetry adapted local minimum

below the symmetry broken minimum, constraint to a C_{2h} geometry. Geometry optimization, under the restriction of both geometry and wave function to C_{2h} symmetry, produces a point ($R_{CC} = 1.91$ Å) that has no connection with the rest of the surface (except with neighbouring C_{2h} adapted solutions), see Fig. 4.

Both RHF and (limited) CASSCF calculations thus reveal discontinuities at the "edge" of the C_{2h} part of the surface. With discontinuous we mean that there are several broken solutions lying below the C_{2h} adapted solution. We now investigate whether our VBSCF functions exhibit the same behaviour. There are several ways to monitor the instability of symmetry adapted solutions. One may look for a lower lying broken solution, but the failure of finding any doesn't prove its non-existence. Therefore, we are following a different path. We perform (symmetry adapted) calculations at a C_{2h} geometry and at a geometry that, by

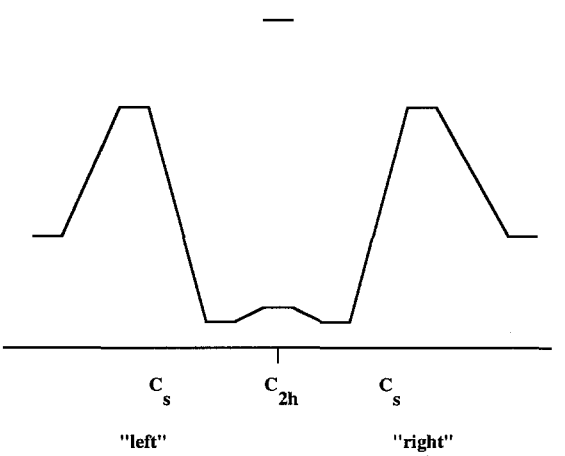

Fig. 4. Schematic representation of the CASSCF potential energy surface of the glyoxal ion

Table 9. Stationary points at the CASSCF potential energy surface

Symmetry	Total energy (a.u.)
C_s [a]	−225.894507
C_s [b]	−225.893323
C_s [c]	−225.895181
C_{2h} [d]	−225.895067
C_{2h} [e]	−225.892686

[a] Local minimum
[b] Saddle point
[c] Global minimum, close to C_{2h} symmetry
[d] Symmetry broken minimum
[e] Symmetry adapted minimum

Table 10. Bond lengths and bond angles (Ångstrom/degrees) at CASSCF stationary points

	C_s [a]	C_s [b]	C_s [c]
R_{CC}	2.050	1.773	1.532
R_{CO1}	1.145	1.187	1.233
R_{CO2}	1.149	1.161	1.191
R_{CH1}	1.079	1.084	1.084
R_{CH2}	1.081	1.075	1.090
θ_{CCO1}	112.1	119.6	121.8
θ_{CCO2}	115.7	113.5	115.1
θ_{CCH1}	107.3	114.0	120.5
θ_{CCH2}	105.0	111.9	118.2

[a] Global minimum
[b] Saddle point
[c] Local minimum

slight alterations to the former, is reduced to C_s symmetry. If the C_{2h} constrained solution is unstable, its energy mismatches the energy at the point of lower symmetry, and a gap will be exposed. Of course, there's always some energy difference noticeable. The inclusion of different methods in the test will, however, reveal which energy differences are acceptable and which point at a discontinuity. As was noted above, the breaking of the symmetry of the wave function depends on the C–C distance. Therefore, the test is performed for both short and long C–C distances (see Table 11). Only VBSCF type 1 was probed; obviously, the higher types will behave properly if type 1 does.

The results confirm that RHF only exhibits a gap for short C–C distance, while CASSCF "breaks" at both distances. The large dipole moments at the skew geometries predict which surfaces are bound to break. In all cases of symmetry breaking, symmetry broken solutions at C_{2h} geometries could be found that matched the energies at the points of lower symmetry. The type 1 surface is

Table 11. Test on the continuity of RHF, CASSCF and VBSCF surfaces on geometric symmetry reduction for both short (A) and long (B) C–C distance[a,b]

	R_{CC} (Å)	Symmetry	Method		
			RHF	CASSCF	VBSCF[c]
A[d]	1.535	C_{2h}	−225.835940	−225.870243	−225.861979
		C_s	−225.873144	−225.891525	−225.861950
			(1.3)	(1.3)	(0.0)
B[d]	2.050	C_{2h}	−225.865062	−225.891174	−225.880774
		C_s	−225.864944	−225.895181	−225.880652
			(0.1)	(0.3)	(0.2)

[a] Total energy in a.u.
[b] For the lower symmetry points, dipole moments (a.u.) are given in parenthesis
[c] VBSCF type 1
[d] Bond lengths and angles of the two points of different symmetry differ in no more than 0.002 Å and 2°, respectively

shown to be continuous in the tested area. Apparently, while using the same active space the VBSCF optimization generates solutions that are stable on symmetry reduction, whereas the CASSCF optimization creates lower solutions that are not. Note that symmetry broken CASSCF solutions at C_{2h} geometries have an active space slightly different from type 1, since its inactive orbitals are of lower symmetry. Some cases of discontinuity on CASSCF potential energy surfaces have been reported before [18].

Despite the correct behaviour of type 1, this method is not free of broken solutions either. That is, given the formal definition of type 1, i.e. two configurations differing in one singly occupied and one doubly occupied orbital, a symmetry broken solution can be found that lies lower than the intended type 1 function. The nature of the former solution differs completely from the latter: Both configurations have their unpaired electron delocalized, with a slight preference for one of the oxygen atoms. One of the structures dominates the wave function, whereas the other is used for dynamical correlation. The explanation for the fact that type 1 nevertheless does not show a gap at geometric symmetry reduction is that lower solutions also exist for C_s symmetry. (The existence of these solutions explain why the RHF energy for C_s symmetry at $R_{CC} = 1.535$ Å lies below type 1 (see Table 11).) So strictly speaking we're not dealing here with a case of *symmetry* breaking. The "broken" solutions do not compensate for an incapability of the model wave function to deal with the unpaired electron, but instead introduce dynamical correlation in the description. Moreover, they are ill defined and converge hardly. Since they do not correspond to our model wave function of two equivalent resonance structures, we reject them. The optimized wave functions that do cope with our model define a potential energy surface that is continuous over a wide range of molecular geometries and is thus reliable enough to serve as a base in a study of the glyoxal ion.

Since TURTLE is not yet integrated in a geometry optimization procedure, we can only present here single point calculations at a selected number of nuclear

geometries. The choice of the geometries is based upon RHF stationary points. First we probe the C–C bond length dependence. The geometries are defined by C_{2h} constrained RHF-optimization of all internal coordinates, while keeping the C–C distance constant. A number of C–C distances is tested, see Table 12. (The largest C–C distance corresponds to the local RHF minimum.) The calculations clearly reveal preference for shorter C–C distances for the more sophisticated wave functions. Regarding the neutral, the C–C bond length of the equilibrium geometry will probably lie around 1.6 Å. The VBSCF functions thus produce a more realistic prediction of the C–C bond length at a C_{2h} geometry than either RHF or CASSCF functions do.

The second series of nuclear geometries used for VBSCF calculations is indicated in Fig. 3 by means of capitals. Point A resembles the geometry with both the skewest molecular skeleton and the shortest C–C distance in the series. The tendency in the sequence of geometries is both in the direction of higher symmetry, i.e. where the left and right part of the molecule are more equivalent, and of longer C–C distance. In point A we have moved far from C_{2h} symmetry, which has several consequences. As stated in Sect. 2, the two structures of the VBSCF functions have equal weights for a C_{2h} geometry. However, lowering the symmetry favours one of the structures: the one fitting best to the present nuclear geometry. During the optimization, the unpaired electron of the minor structure is no longer strictly localized at the unfavourable oxygen atom, but it is still reasonable to regard it as a (minor) resonance structure. Regarding the weights of the configurations, the Mulliken atomic spin populations, and the dipole moments, (not presented), the transition from a double-localized in a mono-localized wave function in going from point E to A evolves first rather slowly, then accelerates near point B, to give a completely mono-localized state at point A. Dipole moments at point B lie around 1.0 a.u.

Of course, the fact that we are mixing two structural parameters into one series of calculations makes the results somewhat hard to interpret. Nevertheless, a few conclusions can be drawn: (See Table 13.) At first, the calculations reveal that the VBSCF surfaces have little in common with RHF or CASSCF surfaces. For instance, along the chosen path on the surface no saddle point appears to be present; and it is safe to say that no saddle point of C_s symmetry exists. Considering also the results presented in Table 12, we find that for each type the lowest points in the two series are found at similar C–C distances. Consequently,

Table 12. RHF and VBSCF total energies at a number of C_{2h} geometries with various C–C distances[a,b]

R_{CC} (Å)	RHF	Type 1	Type 2	Type 3
1.640	−225.854492	−225.876595	−225.892949	−225.915408
1.746	−225.860168	−225.880696	−225.895255	−225.913362
1.852	−225.863489	−225.881966	−225.894942	−225.909554
1.958	−225.865217	−225.881435	−225.893122	−225.904925
2.053	−225.865671	−225.879909	−225.890667	−225.900489

[a] Total energy in a.u.

[b] Nuclear geometries were defined by RHF-optimization of all internal coordinates within C_{2h} symmetry, while keeping the C–C distance fixed

Table 13. RHF and VBSCF total energies (a.u.) for a number of points, illustrated by Fig. 4[a]

Point	R_{CC} (Å)	RHF	Type 1	Type 2	Type 3
A	1.535	−225.876204	−225.881276	−225.888638	−225.914786[b]
B	1.684	−225.870595	−225.881371	−225.894163	−225.915956
C	1.870	−225.863049	−225.882199	−225.895475	−225.910480
D	1.966	−225.864818	−225.881183	−225.892739	−225.904299
E	2.053	−225.865671	−225.879909	−225.890667	−225.900489

[a] Points A, C and E correspond to the RHF C_s global minimum, saddle point and local C_{2h} minimum respectively; B lies geometrically between A and C, whereas D lies between C and E
[b] Considered converged only within 0.5×10^{-3} a.u.

the energy depends more strongly on the length of the C–C bond than on the skewness of the nuclear geometry. Lowering of the symmetry of the ion does not abruptly change the total energy, be it upwards or downwards.

Only two kinds of potential energy surfaces can cope with all achieved results: One in which a C_{2h} geometry is the only minimum and one in which a C_{2h} geometry forms the saddle point between two equivalent C_s minima, see Fig. 5. By simply comparing for the various types the lowest C_{2h} point in the series with the lowest C_s point, we find the C_s minimum to lie lowest always, though the differences are minor (<1 mH). This suggests the "double-well potential" (Fig. 5A) to be most likely, albeit our investigation of the VBSCF surfaces is far from complete. Note that this kind of (double-well) potential is sought after in the examination of the possibility of molecular switches [21, 22]. Note furthermore, both from Tables 12 and 13, that the type 1 potential is very flat. Apparently this type has down leveling qualities. The surfaces grow steeper as the number of breathing orbitals increases, proving that the flatness is just an artefact of type 1.

Finally a comment on CPU times (return to Table 2). The timings reveal the complexity of the calculations and the considerable progression of CPU time with the amount of non-orthogonality caused by the increase in the number of breathing orbitals. In all calculations approximated Newton–Raphson and Direct Inversion of Iterative Subspace (DIIS) are invoked to speed up convergence [29]. In going from symmetric to asymmetric geometries not only the

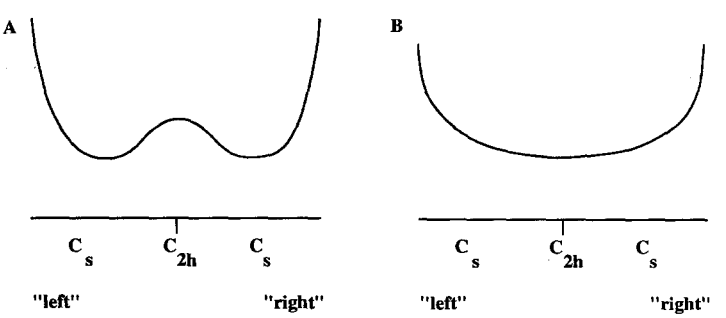

Fig. 5. Two alternative representations of the VBSCF potential energy surface of the glyoxal ion

amount of CPU time per iteration increases, but also the number of iterations needed. Especially at point A of Fig. 3 the VBSCF functions converged very slowly.

6 Conclusions

This work exposes a method that is able to provide a sound description of a radical cation which unpaired electron can be localized at several equivalent atoms. In case of a symmetrical molecular geometry localization of the unpaired electron involves all equivalent sites, whereas for lower symmetry localization takes place at only one site. With the VBSCF method – used in the way shown – both situations can be properly dealt with, and a smooth transition of a "mono-localized" into a "multiple-localized" state is possible. Even the less sophisticated type *breathing* VBSCF function ("type 1") has proved to be stable on symmetry reduction. This is in marked contrast to RHF and CASSCF functions.

A convenient way of looking at the problem of distributing the unpaired electron is in terms of Lewis structures: In this view the difficulty in the description is caused by the competition of several resonance structures. The way to handle this problem is to translate the resonance structures into configurations. At first sight, a primitive but meaningful wave function seems to be formed by two configurations that are interconvertible by single excitation ("type 0"). However, this representation is not useful (and we have proven this numerically), since it is just an unusual representation of the RHF function. *A meaningful representation of the resonance structures is only formed after each configuration is provided with its own active orbitals or, in our terminology, as the active orbitals are allowed to breathe.* This inevitably introduces a non-orthogonality problem, which makes the description expensive. The description can be improved (and the electronic energy can be lowered) systematically by a step-wise increment of the number of breathing orbitals. Mulliken populations of optimized functions have not only shown that each configuration represents a resonance structure (which accounts for type 0 as well), but also that the overall radical character is distributed mainly over the oxygen atoms. All types of VBSCF functions can be converted to orthogonal equivalents, but in most cases this requires excessively large expansions. The use of non-orthogonal orbitals thus confines the size of the expansion and allows for a one-to-one correspondence of configurations with resonance structures.

The successful appliance of breathing orbitals on the glyoxal ion contradicts earlier results on a homonuclear diatom [26]. Here, the breathing orbital recipe was tried at H_2 in an attempt to represent each of the structures H^+H^-, $H-H$ and H^-H^+. This also gives a significant energy lowering relative to a 1-configuration optimization, but the interpretation in terms of the mentioned structures now ceases to exist: In fact, the orbitals reveal a tendency to become orthogonal, whereas for the glyoxal ion the non-orthogonality of the breathing orbitals is essential.

The disadvantage of the model VBSCF functions is that they are best equipped to describe the symmetrical situation, and optimizing them becomes a complicated task for "very asymmetrical" geometries. Furthermore, low lying solutions have been spotted that do not correspond to the model VBSCF functions; instead they introduce dynamical correlation in the description. Fortunately,

the part of the potential energy surface that can be studied without entering into serious problems seems large enough to draw all relevant conclusions.

The configurations used in the VBSCF functions have only one orbital single occupied, and thus no spin-coupling occurs in the wave functions. Thus far, spin-coupling seemed to form the essence of the Valence Bond approach, be it classical or modern. However, in our system the formation and breaking of bonds is not relevant: We have merely been describing a special kind of non-dynamical correlation for which spin-coupling does not seem to be of any importance. As it would unnecessarily complicate our calculations we have not introduced it. We must emphasize that the realization of the VBSCF method was essential to be able to perform our calculations. For instance, in the development of a distinct modern Valence Bond approach, Spin-Coupled VB [36, 37], accent has thus far been put on the above mentioned spin-coupling, and, at the time of writing, TURTLE seems to be the only program capable of doing the calculations shown.

Both the smooth behaviour of the VBSCF functions on symmetry lowering and their dependence on the C–C distance, make it likely that VBSCF provides an impression of the glyoxal radical cation potential energy surface that is much more realistic than those based on either RHF or CASSCF. According to our modest series of calculations, a double-well potential seems most probable. However, to obtain more reliable results, a more flexible basis set than SV 4-31G should be used. Furthermore, (gradient-driven) geometry optimization should be applied to localize the minima; such a procedure will soon be implemented. Dynamical correlation can be incorporated in the description by a non-orthogonal Multi-Reference SDCI calculation, with a 2-configuration reference function that may be of any of the type VBSCF functions treated in this paper. An extension of TURTLE that is able to perform such calculations is about to be realized.

Acknowledgements. The investigations were supported (in part) by the Netherlands Foundation for Chemical Research (SON) with financial aid from the Netherlands Organization for Scientific Research (NWO). The authors are indebted to F. B. van Duijneveldt for stimulating discussions.

References

1. Broer-Braam HB (1981) Localized orbitals and broken symmetry in molecules – Theory and applications to the chromate ion and *para*-benzoquinone, Ph.D. Thesis, University of Groningen
2. Ruttink PJA, Lenthe JHv (1981) J Chem Phys 74:5785
3. Paldus J, Veillard A (1978) Mol Phys 35:445
4. Malrieu J-P (1981) Theor Chim Acta 59:251
5. Davidson ER, Bordon WT (1983) J Phys Chem 87:4783
6. Cook DB (1986) J Chem Soc, Faraday Trans 2 82:187
7. Goscinski O (1986) Int J Quant Chem: Quant Chem Symp 19:51
8. Lepetit M-B, Malrieu J-P, Trinquier G (1989) Chem Phys 130:229
9. Tarantelli F, Cederbaum LS, Campos P (1989) J Chem Phys 91:7039
10. Ruttink PJA (1988) in: Naaman R, Vager Z (eds) The structure of small ions. Plenum, NY
11. Pople JA, Seeger R, Krishnan R (1977) Int J Quant Chem: Quant Chem Symp 11:149
12. Ruttink PJA (unpublished results)
13. Collins JR, Gallup GA (1991) J Mol Str (Theochem) 229:91
14. Broer R, Nieuwpoort WC (1988) Theor Chim Acta 73:405
15. Hollauer E, Nascimento MAC (unpublished)

16. Hollauer E, Nascimento MAC (unpublished)
17. Hollauer E, Nascimento MAC (1991) Chem Phys Lett 184:470
18. Sanchez de Meras A, Lepetit M-B, Malrieu J-P (1990) Chem Phys Lett 172:163
19. Nitzsche LE, Davidson ER (1978) Chem Phys Lett 58:171
20. Hollauer E, Nascimento MAC (1991) Chem Phys Lett 181:463
21. Hush NS (1980) in: Brown DD (ed) Proc Conf Mixed-valence compounds – Theory and applications in chemistry, physics and biology (Oxford, 1979). Reidel, Dordrecht
22. Hush NS, Wong AT, Bacskay GB, Reimers JR (1990) J Am Chem Soc 112:4192
23. Ditchfield R, Hehre WJ, Pople JA (1971) J Chem Phys 54:724
24. Lenthe JHv, Balint-Kurti GG (1980) Chem Phys Lett 76:138
25. Lenthe JHv, Balint-Kurti GG (1983) J Chem Phys 78:5699
26. Verbeek J (1990) Nonorthogonal orbitals in *ab initio* many-electron wavefunctions, Ph.D. Thesis, University of Utrecht
27. Verbeek J, Lenthe JHv (1991) J Mol Str (Theochem) 229:115
28. Verbeek J, Lenthe JHv (1991) Int J Quant Chem 40:201
29. Lenthe JHv, Verbeek J, Pulay P (1991) Mol Phys 73:1159
30. Verbeek J, Langenberg JH (1989) TURTLE – an *ab initio* VB/VBSCF/VBCI program, Utrecht
31. Malrieu JP (1989) Planning meeting for the CECAM VB workshop Orsay
32. Voter AF, Goddard III WA (1981) Chem Phys 57:253
33. Dupuis M, Spangler D, Wendoloski JJ (1980) NRCC Program QG01, GAMESS, Lawrence Berkeley Laboratory
34. Guest MF, Kendrick J (1986) GAMESS User manual, Daresbury Laboratory, Daresbury
35. Guest MF, Harrison RJ, Lenthe JHv, Corler LCHv (1987) Theor Chim Acta 71:117
36. Cooper DL, Gerratt J, Raimondi M (1987) in: Lawley KP (ed) Ab Initio Methods in Quantum Chemistry-II, Adv Chem Phys 59, Wiley, NY
37. Cooper DL, Gerratt J, Raimondi M (1988) Int Rev Phys Chem 7:59